Excited-state geometries and vibrational frequencies studied using the analytical energy gradients of the direct symmetry-adapted cluster–configuration interaction method. I. HAX-type molecules

Masahiro Ehara,[1,a)] Fumito Oyagi,[2] Yoko Abe,[2] Ryoichi Fukuda,[1] and Hiroshi Nakatsuji[2,3,4,a)]

[1]*Institute for Molecular Science, 38 Nishigonaka, Myodaiji, Okazaki 444-8585, Japan*
[2]*Department of Synthetic Chemistry and Biological Chemistry, Kyoto University, Katsura, Kyoto 615-8510, Japan*
[3]*Quantum Chemistry Research Institute, Goryo Oohara 1-36, Nishikyo-ku, Kyoto 615-8245, Japan*
[4]*JST, CREST, Sanboncho-5, Chiyoda-ku, Tokyo 102-0075, Japan*

(Received 30 March 2011; accepted 6 July 2011; published online 29 July 2011)

In this series of studies, we systematically apply the analytical energy gradients of the direct symmetry-adapted cluster–configuration interaction singles and doubles nonvariational method to calculate the equilibrium geometries and vibrational frequencies of excited and ionized states of molecules. The harmonic vibrational frequencies were calculated using the second derivatives numerically computed from the analytical first derivatives and the anharmonicity was evaluated from the three-dimensional potential energy surfaces around the local minima. In this paper, the method is applied to the low-lying valence singlet and triplet excited states of HAX-type molecules, HCF, HCCl, HSiF, HSiCl, HNO, HPO, and their deuterium isotopomers. The vibrational level emission spectra of HSiF and DSiF and absorption spectra of HSiCl and DSiCl were also simulated within the Franck–Condon approximation and agree well with the experimental spectra. The results show that the present method is useful and reliable for calculating these quantities and spectra. The change in geometry in the excited states was qualitatively interpreted in the light of the electrostatic force theory. The effect of perturbation selection with the localized molecular orbitals on the geometrical parameters and harmonic vibrational frequencies is also discussed. © *2011 American Institute of Physics*. [doi:10.1063/1.3617233]

I. INTRODUCTION

Electronic properties, geometric structures, and spectroscopic constants in molecular excited states are of interest because they are characteristics compared with those in the ground states. Recent developments in high-resolution spectroscopy have enabled us to obtain precise information on such quantities. Geometry relaxation and dissociation dynamics in the excited states can be elucidated by analyzing the fine structure arising from the vibrational spectra. Theoretical information is valuable for interpreting these high-resolution spectra and the physics behind them. Thus, the interplay between experiment and theory has become relevant in modern molecular spectroscopy.

Theoretical spectroscopy has been achieved using various electronic structure theories. Peyerimhoff and co-workers performed pioneering work using the multireference singles and doubles configuration interaction (MRSDCI) method.[1] Nakatsuji has developed the symmetry-adapted cluster expansion (SAC)/symmetry-adapted cluster–configuration interaction (SAC–CI) (Refs. 2–4) method to study molecular excited states based on cluster expansion. Multireference cluster-expansion theories have also been developed for quasidegenerate systems.[5] Various types of multireference-type perturbation theories, such as complete-active-space perturbation theory (CASPT2) (Ref. 6) and multireference second-order Møller–Plesset perturbation theory,[7] have also been proposed and applied to molecular excited states. For theories aimed at theoretical spectroscopy, the development of analytical energy gradients is also a relevant issue because the derivatives of the potential energy surfaces (PESs) are key fundamental quantities to investigate the geometries, vibrations, and energy relaxation processes of the excited-state molecules.

The SAC/SAC–CI method has been established for investigating molecular excited states through numerous applications over a wide field of chemistry and physics. The method has been applied to molecular spectroscopy, biological chemistry, material science, and surface photochemistry.[4,8] The analytical energy gradients of the SAC/SAC–CI method have also been formulated and implemented.[9,10] The method has been applied to the calculation of equilibrium geometries and one-electron properties, such as dipole moments in various electronic states. It should be noted that the SAC–CI analytical energy gradient method is applicable to the higher excited states that cannot be accessed by ground-state theories such as quadratic configuration interaction singles and doubles (QCISD) (Ref. 11) and CCSD(T).[12]

The analytical energy gradients of the SAC/SAC–CI method have been applied to the geometry optimization

a)Authors to whom correspondence should be addressed. Electronic addresses: ehara@ims.ac.jp and h.nakatsuji@qcri.or.jp.

of molecules in excited, ionized, electron-attached, and high-spin states.[8,10] Although this approach is useful for calculating force constants and vibrational frequencies, the method has not been utilized for this purpose. Behind this, there is one central issue: accurate calculation of the PESs and the energy derivatives is necessary to guarantee the reliability of the calculations of these quantities. In the SAC–CI method, we use the perturbation-selection approach,[13] which is effective for large-scale calculations; however, this may involve the possibility of introducing an inaccuracy in calculating vibrational frequencies. Recently, a direct algorithm for the SAC/SAC–CI method has been developed,[14] and the calculation of all the necessary product operators without any selection has become possible. This method is expected to be useful in calculating the vibrational frequencies.

Taking account of these issues in this series of studies, we systematically investigate the excited-state geometries and vibrational frequencies of the valence and core-excited/ionized states using the analytical energy gradients of the direct SAC/SAC–CI method at the singles and doubles (SD–*R*) level. We examine the various electronic states in singlet, doublet, and triplet spin multiplicities that can be calculated by the direct SAC–CI method and its analytical energy gradients. Therefore, we have selected electronic states that have been well studied by both experiments and theories. We have also calculated some higher electronic and vibrationally excited states that have not been examined so far.

The vibrational energy levels and the Franck–Condon (FC) factors between the different electronic states have also been extensively investigated based on accurate *ab initio* PESs. For small systems, such as triatomic molecules, the grid method is a straightforward and powerful approach to calculating the vibrational energy levels and FC factors. Recently, postvibrational self-consistent field theories, such as vibrational configuration interaction (VCI),[15] vibrational Møller–Plesset perturbation,[16] and vibrational coupled-cluster[17] methods have been developed for calculating the vibrational levels of polyatomic molecules. An efficient approach known as the scaled hypersphere search method[18] has also been developed. In all of these methods, accurate calculation of the PESs is the most relevant issue.

The equilibrium geometries and spectroscopic constants of excited states of triatomic molecules have been extensively studied and much experimental data have been accumulated. Recently, accurate spectroscopic constants have been determined for HSiF (DSiF) (Refs. 19 and 20) and HSiCl (DSiCl) (Refs. 21 and 22) using high-resolution single vibronic level (SVL) emission spectroscopy and laser induced fluorescence (LIF) spectroscopy. Accurate theoretical calculations of the absorption and emission spectra were also performed for these molecules.[23,24] The HCF,[25] HCCl,[26,27] and HAO (A = N, P) (Ref. 28) molecules that have isovalence electronic structures to HSiX (X = F, Cl) were also investigated by some experimental and theoretical studies. These molecules show characteristic geometry changes in the excited states and their spectroscopic constants have been intensively investigated for several electronic states and, therefore, the excited states of these molecules are good benchmarks for the present study.

Thus, in this work, we applied the direct SAC–CI method and its analytical energy gradients to the valence excited states of triatomic monohydrides, HCX (X = F, Cl), HSiX (X = F, Cl), and HAO (A = N, P), and their deuterium isotopomers to calculate the excited-state equilibrium geometries, vibrational frequencies, and adiabatic excitation energies. The harmonic vibrational frequencies have been numerically calculated using the analytical first derivatives and the anharmonicities have been evaluated using the three-dimensional (3D) PESs around the local minima. The vibrational level emission spectra of HSiF and DSiF and absorption spectra of HSiCl and DSiCl were also simulated within the FC approximation. The geometry change in the excited states is qualitatively interpreted based on the electrostatic force (ESF) theory.[29] Perturbation selection with the localized molecular orbitals (LMOs) combined with the minimum-orbital deformation (MOD) method[30] is also examined for calculating the excited-state equilibrium geometries and harmonic vibrational frequencies.

II. COMPUTATIONAL DETAILS

All of the geometry optimizations for the valence excited states were performed by the analytical energy gradients with the direct SAC–CI SD–*R* nonvariational method. The vibrational analysis was performed at the stationary points and the harmonic vibrational frequencies were calculated with the second derivatives numerically computed from the analytical first derivatives. The zero-point energy correction was performed for calculating the adiabatic excitation energies, T_0. In the present results, all of the geometrical parameters are given as r_e and θ_e, not as r_0 and θ_0.

The ground and valence excited states of triatomic monohydrides with singlet and triplet spin multiplicities were calculated; namely, the ground, singlet, and triplet excited states (X^1A', A^1A'', a^3A'') of HCX (X = F, Cl), HSiX (X = F, Cl), and HAO (A = N, P). The basis set dependence of the equilibrium geometries and T_0 was examined for HSiF with Dunning's correlation-consistent polarized valence double zeta (cc-pVDZ), cc-pVTZ, and cc-pVQZ basis sets,[31] without f- and g-type polarization functions for Si and F and without d- and f-type polarization functions for H. These basis sets are denoted as cc-pVTZ–f and cc-pVQZ–f,g in the present paper. The basis set examination showed that cc-pVTZ-f provides reasonable results at an acceptable computational cost and, therefore, the calculations of other molecules were performed with the cc-pVTZ–f basis sets [4*s*3*p*2*d*/3*s*2*p*/5*s*4*p*2*d*].

In the SAC–CI calculations, the direct algorithm of the SAC–CI SD–*R* method[14] has been utilized without perturbation selection of the linked operators to calculate the valence excited states. The SD–*R* method has been shown to describe the excited states accurately when the excited states are predominantly described by one-electron processes. The recently developed direct SAC–CI method enables accurate and efficient calculations. This direct SAC–CI method calculates all the product terms of S_2S_2, S_2R_1, and S_2R_2 without selection, where S_2 denotes linked double operators in SAC and R_1 and R_2 are linked single and double operators in SAC–CI, respectively. All of the direct SAC–CI calculations were performed by the nonvariational method, which is the default in

the program system. Recently, the analytical energy gradients of the direct SAC–CI method have also been developed and implemented.

To reduce the computational cost of calculating the ground- and excited-state geometries and harmonic vibrational frequencies, a method incorporating perturbation selection has been examined. The LMOs calculated by Pipek–Mezey population localization[32] were used. The MOD method[30] was adopted in the geometry optimizations and the calculations of the first derivatives and Hessian matrices. The set of excitation operators were fixed in the calculations of the first and second derivatives for obtaining smooth PESs. The perturbation selection[13] was performed with some energy thresholds, $(\lambda_g, \lambda_e) = (10^{-7}, 10^{-8})$, etc., for the double excitation operators, S_2 and R_2 operators, respectively.

For evaluating the anharmonic vibrational frequencies, the 3D PESs were calculated around the local minima with 343 geometric points (seven cubic points) to cover the region of the 3D vibrational wavefunctions. The 3D PESs were described in the binding coordinates (r_1, r_2, θ), where r_1 and r_2 are the bond distances and θ defines the bond angle. For calculating the vibrational wavefunctions, these energy points were fitted with the 3D fifth-order Morse–cosine function,

$$V(r_1, r_2, \theta) = \sum_{i,j,k=0}^{5} B_{ijk}(1 - e^{-a_1(r_1 - r_{e_1})})^i \times (1 - e^{-a_2(r_2 - r_{e_2})})^j (\cos\theta - \cos\theta_e)^k, \quad (1)$$

where r_{e_1}, r_{e_2}, and θ_e are the equilibrium values. The linear parameters $\{B_{ijk}\}$ were obtained by a least-square fitting with varying of the nonlinear parameters (a_1, a_2). The fitting of the 3D PES was satisfactory and the mean deviation from the *ab initio* values at 343 geometric points was 0.1–0.6 cm^{-1} for all the electronic states of the present molecules. This 3D PES expansion guarantees accurate calculations of the vibrational energy levels and wavefunctions, including anharmonicity.

For simulating the vibrational spectrum, 3D vibrational states were calculated by the grid method, in which the Lanczos algorithm was adopted for the diagonalization. In the binding coordinates, the kinetic part of the Hamiltonian ($J = 0$) of the vibrational motion of the A–B–C system is given by[33]

$$T = \frac{p_1^2}{2\mu_{AB}} + \frac{p_2^2}{2\mu_{BC}} + \frac{j^2}{2\mu_{AB}r_1^2} + \frac{j^2}{2\mu_{BC}r_2^2} + \frac{p_1 p_2 \cos\theta}{m_B} - \frac{p_1 p_\theta}{m_B r_2} - \frac{p_2 p_\theta}{m_B r_1} - \frac{\cos\theta j^2 + j^2 \cos\theta}{2m_B r_1 r_2}, \quad (2)$$

where

$$p_k = -i\frac{\partial}{\partial r_k}, \quad k = 1, 2, \quad p_\theta = -i\frac{\partial}{\partial\theta}\sin\theta$$
$$j^2 = -\frac{1}{\sin\theta}\frac{\partial}{\partial\theta}\sin\theta\frac{\partial}{\partial\theta}, \quad (3)$$

and μ_{AB} and μ_{BC} are the reduced masses of the A–B and B–C systems, respectively. The coordinates r_1 and r_2 are represented by the Hermite discrete variable representation (DVR) with 30 points and θ by the Legendre DVR of 19 points. Thus, the 3D vibrational wavefunction is represented at the grid points,[34]

$$x_j(x) = (2^j j!)^{-1/2}(m\omega/\pi)^{1/4} H_j(\sqrt{m\omega}(x - \tilde{x}))e^{-m\omega(x-\tilde{x})^2/2}, \quad (4)$$

$$\chi_{l-m+1}(\theta) = \sqrt{\frac{2l+1}{2}\frac{(l-m)!}{(l+m)!}} P_l^m \cos(\theta). \quad (5)$$

The FC factors were calculated using the 3D vibrational wavefunctions.

The SAC/SAC–CI calculations were conducted using the GAUSSIAN09 suite of programs, Revision B.01.[35] The vibrational wavefunctions were calculated with the MCTDH program package, version 8.3.[34]

III. VALENCE EXCITED STATES

A. Structure of HAX (A = C, Si; X = F, Cl) in the ground and excited states

First, the equilibrium structures of the X^1A', A^1A'', and a^3A'' states of HSiF, whose valence electronic structure in the ground state is $\ldots(8a')^2(2a'')^2(9a')^2(10a')^2(3a'')^0$, have been calculated to examine the basis set dependence for the geometrical parameters and adiabatic excitation energies (T_0). The cc-pVDZ, cc-pVTZ–f, and cc-pVQZ–f,g basis sets have been examined and the results are compared in Table I together with the available experimental values.[19] The ground-state structure was obtained as $r_{HSi} = 1.526$ Å, $r_{SiF} = 1.616$ Å, and $\theta = 96.7°$ with cc-pVQZ–f,g in good agreement with the experimental values of $r_{HSi} = 1.528$ Å, $r_{SiF} = 1.603$ Å, and $\theta = 96.9°$, respectively.[19] The low-lying excited states, A^1A'' and a^3A'', are characterized as a $10a' \rightarrow 3a''$ transition that is $n\pi^*$ in character. In the excited states, the prominent geometry change occurs in the bond angle; the bond angle of A^1A'' is enlarged to 115.2°, which is also in good agreement with the experimental value of 115.0°.[19] The bond lengths in the A^1A'' state were predicted to shrink, in agreement with experiment. The calculated T_0 of the A^1A'' state is 2.974 eV compared with the experimental value of 2.884 eV.[19] The agreement with the experimental values in both geometrical parameters and T_0 generally improves as the quality of the basis set improves. For the a^3A'' state, a large geometry change from the ground state has also been calculated for the bond angle (114.2°) and the r_{HSi} bond length (1.484 Å). The bond angle in a^3A'' is similar to that in A^1A'', while r_{HSi} in a^3A'' is much shorter than r_{HSi} in A^1A''. This state has been calculated to be located at 1.612 eV relative to the ground state. Unfortunately, there are no experimental data for this state. The results using the cc-pVTZ–f basis set are also satisfactory compared with those using the cc-pVQZ–f,g basis set; the deviations are <0.012 Å in bond length, <0.4° in bond angle, and <0.013 eV in T_0 for the ground and excited states of HSiF, as in Table I. The moderate deviation of the calculated r_{SiF} values from the experimental ones can be partly attributed to the slow convergence of electron correlation with respect to angular momentum in the basis set; f and g functions were not included in the present calculations.

TABLE I. Geometries and adiabatic excitation energies (eV) of HSiF calculated by the direct SAC–CI SD–*R* method; basis set dependence.

State	Method	Basis set[a]	r_{HSi} (Å)	r_{SiF} (Å)	Θ (°)	T_0
X^1A'	SAC	cc-pVDZ	1.540	1.664	96.7	...
		cc-pVTZ–f	1.533	1.626	96.7	...
		cc-pVQZ–f,g	1.526	1.616	96.7	...
	Expt. (r_e,θ_e)[b]		1.528(5)	1.603(3)	96.9(5)	...
A^1A''	SAC–CI	cc-pVDZ	1.548	1.670	113.8	3.037
		cc-pVTZ–f	1.533	1.625	114.8	3.000
		cc-pVQZ–f,g	1.522	1.613	115.2	2.974
	Expt. (r_e,θ_e)[b]		1.526(14)	1.597(3)	115.0(6)	2.884
a^3A''	SAC–CI	cc-pVDZ	1.498	1.664	114.6	1.637
		cc-pVTZ–f	1.491	1.622	114.1	1.625
		cc-pVQZ–f,g	1.484	1.619	114.2	1.612

[a]cc-pVTZ–f and cc-pVQZ–f,g denotes cc-pVT(Q)Z basis sets without f and g functions for Si and F and without d and f functions for H.
[b]Reference 19. The uncertainty in a structural parameter given in parentheses applies to the last significant figures as usual; e.g., 1.528(5) Å = 1.528 ± 0.005 Å.

Because the calculations with cc-pVTZ–f have provided relatively well-converged results in the basis set examination for HSiF, we performed the calculations of the spectroscopic constants of other molecules with the cc-pVTZ–f basis set. The results for the geometric parameters for the X^1A', A^1A'', and a^3A'' states of HAX (A = C, Si; X = F, Cl) with the cc-pVTZ–f basis set are summarized in Table II comparing with other theoretical and experimental values. Because these four molecules have isovalence electronic structures, the geometry changes in the excited states are similar; the HA and AX bond lengths shrink and the bond angle becomes larger in the excited states. For HCF, Schmidt *et al.* determined the spectroscopic constants of the X^1A', A^1A'', and a^3A'' states using multireference configuration interaction (MRCI) calculations with cc-pVTZ and cc-pVQZ followed by Davidson correction.[25] The present SAC–CI calculation provides results of similar quality to the MRCI calculation compared with the experimental values of the X^1A' (Ref. 36) and A^1A'' states;[37,38] the deviations from experimental values are within 0.03 Å for r_{HC}, 0.004 Å for r_{CF}, and 0.8° for θ. For a^3A'', the SAC–CI calculation also supported the previous calculation; for example, the bond angle is smaller than that of A^1A''.[25] The calculated T_0 values of the A^1A'' and a^3A'' states are 2.215 and 0.542 eV, respectively, and the experimental value of A^1A'' is 2.142 eV. For HCCl, although experimental[39,40] and other theoretical[26,27] works have been reported, information on the A^1A'' and a^3A'' states is limited. The present SAC–CI method has calculated the adiabatic excitation energy of the A^1A'' state as 1.607 eV compared with the observed value of T_0 = 1.524 eV.[40] The a^3A'' state is located very close to the ground X^1A' state (T_0 = 0.149 eV). A MP2 study has been reported for the X^1A' and a^3A'' states.[26] Our results are similar to the MP2 values for bond angle; however, the CCl bond distance is longer by 0.017 Å. For HSiF, the present calculation has yielded satisfactory results compared with the experimental values[19,23] as discussed above and gave results of similar quality to the CCSD(T) with aug-cc-pVQZ for X^1A' and the complete-active-space self-consistent field (CASSCF)/MRCI with aug-cc-pVQZ for A^1A''.[23] This means the effect of the triple correction is small for the ground-state geometrical parameters of this molecule. The present calculations also gave excellent results for HSiCl; deviations from the experimental values[22,41] are within 0.01 Å for r_{HSi}, 0.04 Å for r_{SiCl}, and 0.6° for θ for the X^1A' and A^1A'' states. For the A^1A'' states, density functional theory calculations with B3LYP/6–311G(3*df*,3*pd*) also gave results of similar quality. The calculated T_0 of A^1A'' was 2.679 eV compared with the experimental value of 2.569 eV.

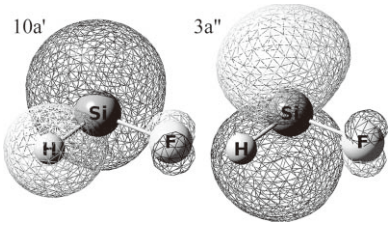

FIG. 1. The isosurfaces of 10a′ and 3a″ MOs of HSiF for the ground-state geometry.

Thus, in the present calculations, for the halocarbenes and halosilenes (HAX), the agreement with the experimental values for the X^1A' and A^1A'' states is satisfactory; the average discrepancies of the geometric parameters between theoretical and available experimental values are 0.012 Å, 0.022 Å, and 0.4° for r_{HA}, r_{AX}, and θ, respectively. The adiabatic excitation energies have also been well reproduced; the mean deviation from the experimental values is 0.096 eV. Because these excited states are described by one-electron processes, the SD–*R* method describes these excited states satisfactorily. The less accurate results in bond lengths (r_{AX}), in particular for HSiF and HSiCl, can be attributed to the quality of the basis set. As we have demonstrated for HSiF in Table I, the higher basis set such as cc-pVQZ-f,g improves the results, however, the systematic calculations including vibrational frequency are practically too expensive with higher basis sets.

The geometry change in the excited states can be qualitatively interpreted with the ESF theory.[29] Because the geometry changes in the excited states of HCX and HSiX are similar, the changes in HSiF have been analyzed. The MOs related to the transition are shown in Fig. 1. Figure 2 shows the contour plot of the electron density difference between the X^1A' and A^1A'' states in the molecular plane (σ_h plane), where the effective density matrices (EDMs) of the SAC/SAC–CI energy gradients were used with the cc-pVTZ–f basis at the ground-state geometry. The contour value denotes EDM(A^1A'')−EDM(X^1A') and, therefore, the negative value means that the electron density is reduced because of the electron excitation. As mentioned above, in the A^1A'' state, the prominent geometry change occurs in the bond angle; θ = 96.7° in X^1A' is enlarged to θ = 114.8° in A^1A''. Figures 1 and 2 show that the nπ^* transition reduces an atomic dipole (AD) force in the molecular plane acting on the Si atom, which causes the bond angle to increase. A similar electron density change occurs in the a^3A'' state and also in the excited states of the other molecules.

TABLE II. Geometries and adiabatic excitation energies (eV) of HAX (A = C, Si; X = F, Cl) calculated by the direct SAC–CI SD–*R* method with cc-pVTZ–f basis sets. The uncertainty in a structural parameter given in parentheses applies to the last significant figures.

Molecule	State	Method	r_{HA} (Å)	r_{AX} (Å)	Θ (°)	T_0
HCF	X^1A'	MRCI+Dav.[a]	1.123	1.319	102.0	…
		SAC	1.119	1.310	102.2	…
		Expt. (r_e,θ_e)[b]	1.130(3)	1.305(3)	103.0(5)	…
	A^1A''	MRCI+Dav.[a]	1.099	1.311	124.5	2.110
		SAC–CI	1.095	1.304	124.2	2.215
		Expt. (r_0,θ_0)[c,d]	1.063(13)	1.308(6)	123.8(8)	2.142
	a^3A''	MRCI+Dav.[a]	1.087	1.324	121.7	0.571
		SAC–CI	1.085	1.318	121.2	0.542
HCCl	X^1A'	MP2[e]	1.103	1.689	102.8	…
		SAC	1.106	1.715	101.9	…
		Expt. (r_s,θ_s)[f]	1.1188(71)	1.6961(25)	101.4(12)	…
	A^1A''	SAC–CI	1.083	1.653	130.1	1.607
		Expt.[g]	…	…	134(5)	1.524
	a^3A''	MP2[e]	1.078	1.668	126.2	…
		SAC–CI	1.080	1.685	125.7	0.149
HSiF	X^1A'	CCSD(T)[h]	1.529	1.613	96.7	…
		SAC	1.533	1.626	96.7	…
		Expt. (r_e,θ_e)[i]	1.528(5)	1.603(3)	96.9(5)	…
	A^1A''	CASSCF/MRCI[h]	1.522	1.619	116.7	…
		SAC–CI	1.532	1.625	114.8	3.000
		Expt. (r_e,θ_e)[i]	1.526(14)	1.597(3)	115.0(6)	2.884
	a^3A''	SAC–CI	1.491	1.622	114.1	1.625
HSiCl	X^1A'	DFT[j]	1.525	2.096	94.8	…
		SAC	1.523	2.107	95.2	…
		Expt. (r_e,θ_e)[j]	1.515(2)	2.0700(3)	95.0(1)	…
	A^1A''	DFT[j]	1.501	2.096	115.5	…
		SAC–CI	1.518	2.083	116.7	2.679
		Expt. (r_e,θ_e)[k]	1.510(10)	2.0465(14)	116.1(8)	2.569
	a^3A''	SAC–CI	1.489	2.079	115.3	1.433
Mean deviations from expt.			0.012	0.022	0.4	0.096

[a]Reference 25.
[b]Reference 36.
[c]Reference 37.
[d]Reference 38.
[e]Reference 26.
[f]Reference 39.
[g] Reference 40.
[h]Reference 23.
[i]Reference 19.
[j]Reference 22.
[k]Reference 41.

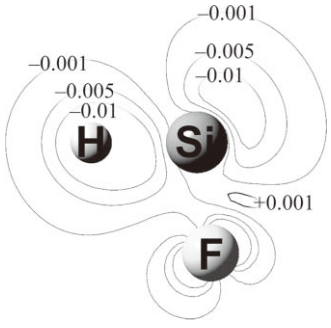

FIG. 2. The contour plot of the electron density difference between X^1A' and A^1A'' states of HSiF for the ground-state geometry.

B. Harmonic and anharmonic vibrational frequencies of HAX (A = C, Si; X = F, Cl)

The vibrational frequencies of HAX (A = C, Si; X = F, Cl) and their deuterium isotopomers have been investigated. In Table III, the calculated harmonic (ω) and anharmonic (ν) vibrational frequencies of the X^1A', A^1A'', and a^3A'' states of the HAX molecules are compared with the experimental[19,21,36,42–44] and other theoretical values. The high-resolution vibrational spectra of the X^1A' and A^1A'' states of HSiX (X = F, Cl) were measured by single vibronic level emission spectroscopy and the harmonic frequencies were extracted.[20,22,23] For the harmonic frequencies, the present theoretical values show reasonable agreement with

TABLE III. Harmonic and anharmonic vibrational frequencies of the ground and excited states of HAX (A = C, Si; X = F, Cl) calculated by the SAC–CI SD–*R* method with cc-pVTZ–f basis sets.

Mol.	State	Method	ω_1(HA)	ω_2(bend)	ω_3(AX)	ν_1(HA)	ν_2(bend)	ν_3(AX)
HCF	X^1A'	MRCI+Dav.[a]	2799	1435	1198	–	–	–
		SAC	2799	1469	1229	2655	1424	1205
		Expt. (gas)[b]	–	–	–	2643	1403	1204
	A^1A''	MRCI+Dav.[a]	3042	1041	1292	2698	1007	1260
		SAC–CI	2997	1055	1292	2791	1022	1266
		Expt. (gas)[c]	–	–	–	–	1021	–
	a^3A''	MRCI+Dav.[a]	3199	1128	1277	–	–	–
		SAC–CI	3153	1147	1270	3007	1125	1248
HCCl	X^1A'	SAC	2942	1248	797	2800	1223	785
		Expt. (gas)[d]	–	–	–	2800	1201	810
	A^1A''	SAC–CI	3166	914	896	3006	882	878
		Expt. (gas)[d]	–	–	–	–	865	–
	a^3A''	SAC–CI	3210	1003	859	3077	972	849
HSiF	X^1A'	SAC	2003	881	839	1928	867	829
		Expt. (gas)[e]	2009	876	831	1932	858	838
		Expt. (Ar)[f]	–	–	–	1913	859	834
	A^1A''	SAC–CI	1797	592	844	1566	557	832
		Expt. (gas)[g]	1816	597	868	1547	558	857
	a^3A''	SAC–CI	2149	691	859	2043	674	849
HSiCl	X^1A'	SAC	2047	822	512	1970	810	507
		Expt. (gas)[e]	2044	822	529	–	808	522
	A^1A''	SAC–CI	1923	583	521	1749	558	512
		Expt. (gas)[c]	–	564	533	1756	568	533
	a^3A''	SAC–CI	2166	659	538	2068	642	531

[a]Reference 25.
[b]Reference 36.
[c]Reference 42.
[d]Reference 43.
[e]Reference 22.
[f]Reference 44.
[g]Reference 19.

the experimental values; the deviations from the experimental values are 5–24 cm^{-1} and 0–19 cm^{-1} for HSiF and HSiCl, respectively. In HSiF, the harmonic frequency of the bending coordinate ω_2 becomes smaller in both the A^1A'' (592 cm^{-1}, expt. 597 cm^{-1}) and a^3A'' (691 cm^{-1}) states compared with the X^1A' state (881 cm^{-1}, expt. 876 cm^{-1}); the PESs of the excited states become flat in this coordinate because the AD force decreases. In the A^1A'' state, ω_1 is drastically reduced (1797 cm^{-1}), but ω_3 does not change so much (844 cm^{-1}), which agrees well with the experimental observation (ω_1 = 1816 and ω_3 = 868 cm^{-1}).[19] In the a^3A'' state, on the other hand, both ω_1 and ω_3 have been predicted to become larger than those of the X^1A' state and ω_2 is reduced, as in the A^1A'' state. For HSiCl, the same trend as seen in HSiF has been observed in the calculated harmonic frequencies. The calculated harmonic frequencies of HSiCl show good agreement with the experimental values for the X^1A' (Ref. 22) and A^1A'' states;[22,41] the mean deviation from the experimental values was ~10 cm^{-1}.

The trend in the anharmonic vibrational frequencies of these electronic states is similar to those of the harmonic frequencies. The anharmonicity of the vibrational frequencies is large in the stretching ν_1(HSi) mode in both the ground and excited states of HSiX. For example, the calculated vibrational fundamental frequencies, ν_1, of HSiF are 1928 and 1566 cm^{-1} for the X^1A' and A^1A'' states, respectively; the deviations from the harmonic values ω_1 are 75 and 231 cm^{-1}, respectively. The PESs in the bending coordinate are flat and the vibrational frequencies of ν_2 are as small as 557 cm^{-1} (expt. 558 cm^{-1}) for the A^1A'' state, which indicates that accurate analysis with the 3D PESs is necessary for evaluating the anharmonicity. In both HSiF and HSiCl, the agreement of the vibrational frequencies with the observed values is satisfactory; the average deviations from the available experimental values are ~11 cm^{-1} for the X^1A' and A^1A'' states of HSiF and HSiCl.

For halocarbenes, the fundamental vibrational frequencies have been reported for the ground states of HCF and HCCl.[36,43] The present calculation provided satisfactory results; for example, the calculated vibrational frequencies of the X^1A' state of HCF are 2655 (ν_1), 1424 (ν_2), and 1205 (ν_3) cm^{-1} compared with the observed values of 2643, 1403, and 1204 cm^{-1}, respectively. Experimental studies of the excited-state vibrational frequencies for these molecules, on the other hand, are limited; only the ν_2 values of A^1A'' observed in the UV spectra have been reported for HCF and HCCl because the vibrational progression is large in this coordinate. The present calculation also reproduced the ν_2 values of the A^1A'' state satisfactorily; the calculated values are 1022 and 882 cm^{-1} for HCF and HCCl, respectively,

compared with the experimental values of 1021 and 865 cm^{-1}. As for the spectroscopic parameters of HCF, MRSDCI calculations with extended basis sets have been reported for the X^1A', A^1A'', and a^3A'' states. From the viewpoint of the harmonic frequencies, the present SAC–CI values show good agreement with those by the MRCI calculation.[25] Comparing the present harmonic values with the vibrational frequencies, the anharmonicity is also significant for ν_1 in the ground and excited states of HCX, as in HSiX. The vibrational frequencies of the bending coordinate, ν_2, are reduced in both the A^1A'' and a^3A'' states.

The vibrational frequencies of DCX (X = F, Cl) and DSiX (X = F, Cl) have also been calculated using the same 3D PESs of HAX; the Born–Oppenheimer (BO) approximation being adopted. The calculated vibrational frequencies are summarized in Table IV together with the experimental values. The trend in the vibrational frequencies of the ground and excited states is the same as those of the HAX molecules in which the BO approximation was adopted. For halocarbenes (DCF and DCCl), the experimental values of the bending mode have been reported. The calculated ν_2 values of 1078 and 790 cm^{-1} for X^1A' and A^1A'' states of DCF compare well with the experimental values of 1046 and 780 $\pm$ 5 cm^{-1}, respectively. For DSiF and DSiCl, high-resolution emission spectroscopy has been applied to provide accurate vibrational levels of the ground state. The present values for X^1A' of DSiF, 1401 (ν_1), 642 (ν_2), and 831 (ν_3) cm^{-1}, are in excellent agreement with the experimental values, 1401 (ν_1), 638 (ν_2), and 840 (ν_3) cm^{-1}, respectively. The vibrational frequencies of the excited states of DSiF and DSiCl have not been well studied experimentally.

TABLE IV. Vibrational frequencies of the ground and excited states of DAX (A = C, Si; X = F, Cl) calculated by the SAC–CI SD–*R* method with cc-pVTZ–f basis sets.

Molecule	State	Method	ν_1(HA)	ν_2(bend)	ν_3(AX)
DCF	X^1A'	SAC	1964	1078	1209
		Expt. (Ar)[a]	...	1046	1183
	A^1A''	SAC–CI	2024	790	1250
		Expt. (gas)[a]	...	780(5)	...
	a^3A''	SAC–CI	2244	865	1231
DCCl	X^1A'	SAC	2086	913	775
		Expt. (gas)[a]	...	805	...
	A^1A''	SAC—CI	2249	669	868
		Expt. (Ar)[a]	...	657	...
	a^3A''	SAC–CI	2274	728	850
DSiF	X^1A'	SAC	1401	642	831
		Expt. (gas)[b]	1401	638	840
		Expt. (Ar)[c]	1387	638	833
	A^1A''	SAC–CI	1178	424	829
	a^3A''	SAC–CI	1493	506	847
DSiCl	X^1A'	SAC	1434	594	503
		Expt.(gas) [b,d]	(1473)	(601)	(525)
	A^1A''	SAC–CI	1297	406	522
		Expt.(gas)[a]	...	409	...
	a^3A''	SAC–CI	1447	452	550

[a]Reference 42.
[b]Reference 22.
[c]Reference 44.
[d]Values in the parentheses are harmonic vibrational frequencies.

C. Vibrational level emission and absorption spectra

The calculated vibrational energies of the lowest 20 vibrational levels and their assignments for HSiF and DSiF are summarized in Table V. Those of other molecules (HCF, HCCl, and HSiCl) and their deuterium isotopomers (DCF, DCCl, and DSiCl) are compiled in the supplementary material of Tables S1–S3.[45] Not all of the vibrational levels were measured in the high-resolution spectrum[19,20] because the vibrational levels in the stretching modes (ν_1, ν_3) are not very excited. These data may help in the detailed assignment in future analyses.

The vibrational spectra in the electronic transition are sensitive to the relative positions of the potential minima in the ground and excited states and the shape of the PESs, which is of interest for the present examination of the accuracy of the SAC/SAC–CI calculation. The SAC/SAC–CI describes the well-balanced PESs of the ground and excited states. Because the high-resolution vibronic level emission spectra have been reported for HSiF and DSiF,[19,20] the vibrational spectra were simulated for these molecules based on the calculated 3D PESs. Theoretical simulations have also been performed previously.[23,24] The calculated vibrational emission spectra from the $A(010)$ and $A(110)$ levels of HSiF and those from the $A(000)$ and $A(010)$ levels of DSiF within the FC approximation are compared with the experimental spectra in Figs. 3 and 4, respectively. The present theoretical spectra satisfactorily reproduce the experimental spectra in both peak position and relative intensity of the vibrational progression. The $A(010)$ and $A(110)$ levels of HSiF are the second and tenth vibrational states; therefore, complex vibrational structures are observed. The present SAC–CI calculations have provided reliable results not only for the main progression based on the bending mode, but also for the small structure due to the stretching modes, as seen in Fig. 3. In the $A(010)$ emission spectra, transitions to the (000) and (010) have large FC factors and the progression of higher $(0n0)$ levels is seen with the peak maximum of (050). This trend agrees well with the experimental spectrum. In the $A(110)$ emission spectra, the transitions overlap and the peaks are assigned as shown in Fig. 3; each peak has two dominant contributions except for (100) and (200) peaks. This feature was not seen in previous work.[20,23] The $A(000)$ and $A(010)$ levels of DSiF are the vibrational ground and first excited states. In the spectra, to cover the energy region of 0–5500 cm^{-1}, calculations up to ~70 vibrational states are necessary. The simulated vibrational spectra are also in excellent agreement with the experimental spectra. The $A(000)$ emission spectrum has a maximum intensity at the (020) level. The $A(010)$ emission spectrum of DSiF is similar to that of HSiF and the peak maximum in the higher levels is at (060), which agrees well with the experimental spectrum. The vibrational progressions in the spectra of both HSiF and DSiF are predominantly due to the bending mode and the structure resulting from the stretching modes is less prominent because the geometry changes are large in the bending mode.

TABLE V. Vibrational levels (ν_1, ν_2, ν_3) of HSiF and DSiF calculated by the SAC–CI 3-D PESs. Energy (E) is given in cm^{-1}.

	X^1A'		A^1A''		a^3A''	
No.	State	E	State	E	State	E
			HSiF			
1	(000)	0	(000)	0	(000)	0
2	(001)	829	(010)	557	(010)	674
3	(010)	867	(001)	832	(001)	849
4	(002)	1650	(020)	1103	(020)	1343
5	(011)	1692	(011)	1385	(011)	1519
6	(020)	1729	(100)	1566	(002)	1689
7	(100)	1928	(002)	1637	(030)	2006
8	(003)	2463	(030)	1654	(100)	2043
9	(012)	2510	(021)	1927	(021)	2185
10	(021)	2551	(110)	2067	(012)	2356
11	(030)	2585	(012)	2157	(003)	2521
12	(101)	2756	(040)	2204	(040)	2660
13	(110)	2782	(101)	2394	(110)	2695
14	(004)	3267	(003)	2457	(031)	2844
15	(013)	3319	(031)	2468	(101)	2891
16	(022)	3365	(120)	2553	(022)	3018
17	(031)	3403	(022)	2661	(013)	3184
18	(040)	3438	(050)	2742	(050)	3305
19	(102)	3577	(111)	2888	(004)	3342
20	(111)	3606	(013)	2919	(120)	3344
			DSiF			
1	(000)	0	(000)	0	(000)	0
2	(010)	642	(010)	424	(010)	506
3	(001)	831	(001)	829	(001)	847
4	(020)	1285	(020)	842	(020)	1010
5	(100)	1401	(100)	1178	(011)	1350
6	(011)	1473	(011)	1249	(100)	1493
7	(002)	1654	(030)	1256	(030)	1510
8	(030)	1914	(110)	1574	(002)	1685
9	(110)	2033	(002)	1649	(021)	1850
10	(021)	2113	(021)	1657	(110)	1989
11	(101)	2231	(040)	1669	(040)	2009
12	(012)	2295	(101)	1963	(012)	2185
13	(003)	2469	(120)	2002	(101)	2340
14	(040)	2566	(012)	2054	(031)	2347
15	(120)	2663	(031)	2067	(120)	2482
16	(031)	2746	(050)	2080	(050)	2494
17	(200)	2768	(200)	2238	(003)	2516
18	(111)	2861	(111)	2344	(022)	2682
19	(022)	2933	(130)	2395	(111)	2832
20	(102)	3052	(003)	2452	(041)	2842

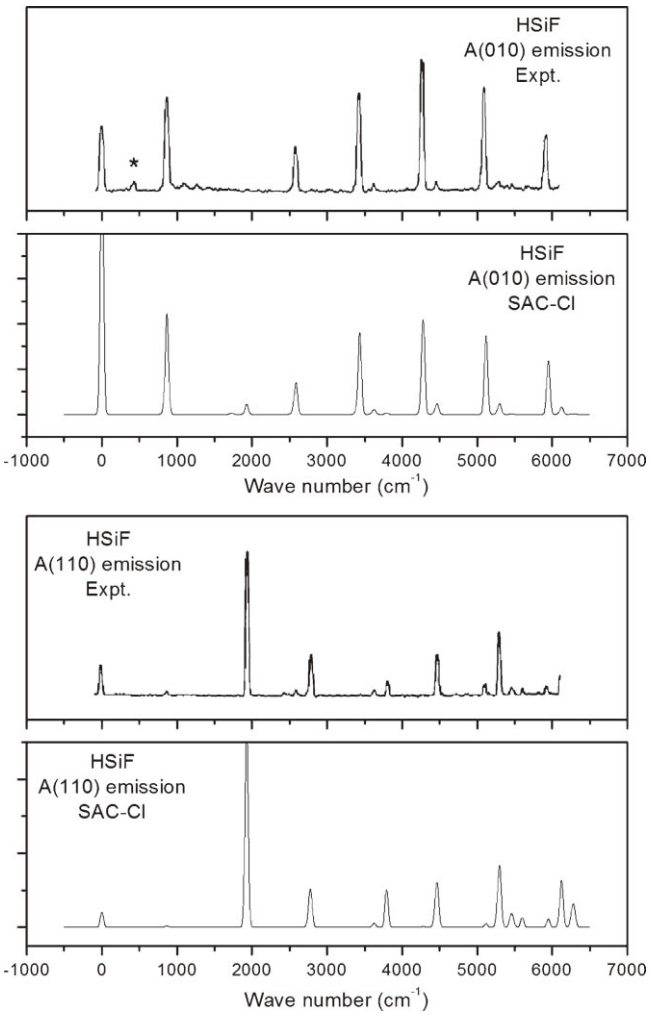

FIG. 3. The SAC–CI $A(010)$ and $A(110)$ emission spectra of HSiF compared with the observed SVL emission spectra (Ref. 20).

The vibrational structure in the absorption spectrum shows vibrational levels in the excited states that are also of particular interest in the present study. The LIF spectra of HSiCl and DSiCl molecules were measured for the X^1A'–A^1A'' transition.[21] Recently, highly accurate calculations of the vibrational level absorption spectra of these molecules were performed using the RCCSD(T) and CASSCF/MRCI methods.[24] In this simulation, they also considered the thermal distribution in the ground state at 300 K. In the present calculation, we focus on the vibrational level absorption spectra from the vibrational ground state and do not include the thermal effect. In Fig. 5, the vibrational level absorption spectra of HSiCl and DSiCl are compared with the LIF spectra[21] in the energy region of 20 600–22 200 cm^{-1}. The present SAC–CI vibrational level absorption spectra agree well with those in the experimental LIF spectra[21] and the previous calculations.[24] In the spectra of HSiCl, the vibrational progression of the bending mode is predominant and the FC factors for 2_0^1 and 2_0^2 are large. The FC factors for other vibrational states, 3_0^1, 3_0^2, $2_0^1 3_0^1$, were calculated to be small. The thermal state in the ground state, $1_1^1 2_0^1$, $1_1^1 2_0^2$, measured in the LIF spectra are not considered in the present calculation. The present calculation also reproduced the vibrational structure in the absorption LIF spectra of DSiCl. The vibrational progression in the bending mode, 2_0^1, 2_0^2, 2_0^3, is prominent and the FC factors of the $2_0^1 3_0^1$, $2_0^2 3_0^1$ transitions are also large. Comparing low-lying peaks, the order of some peaks is different between HSiCl and DSiCl. For example, the peak 2_0^1 lies below 3_0^1 in DSiCl, while their order is reversed in HSiCl. This is because the vibrational frequency ν_3 is smaller than ν_2 in HSiCl and the isotope effect is significant in bending coordinate (ν_2), but is small in stretching coordinate (ν_3) and therefore, the order of these peaks is reversed between HSiCl and DSiCl. The detailed vibrational energy levels of HSiCl

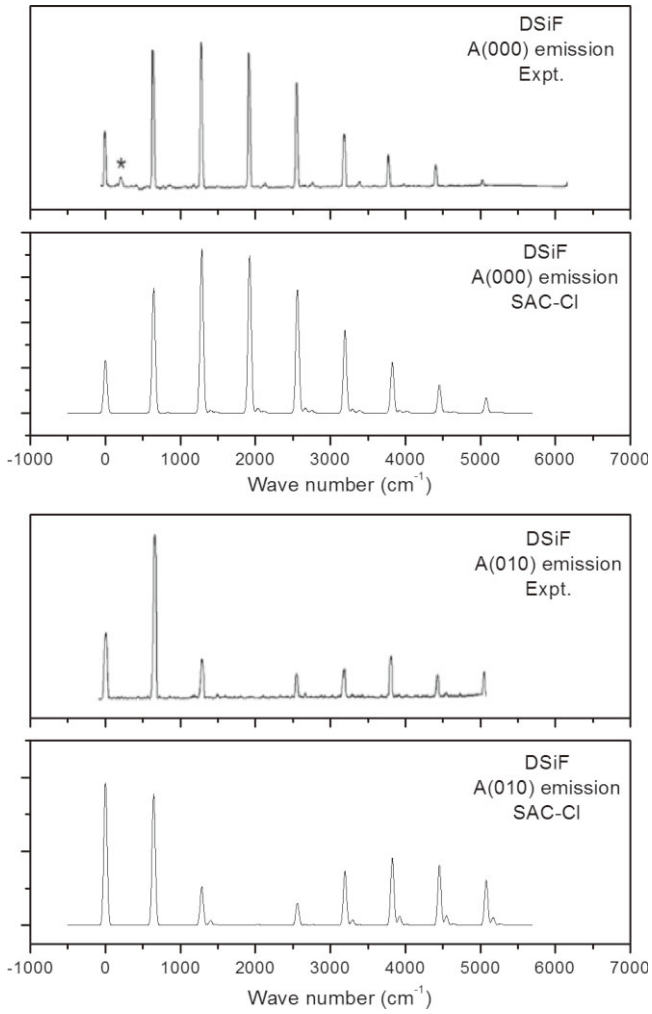

FIG. 4. The SAC–CI $A(000)$ and $A(010)$ emission spectra of DSiF compared with the observed SVL emission spectra (Ref. 20).

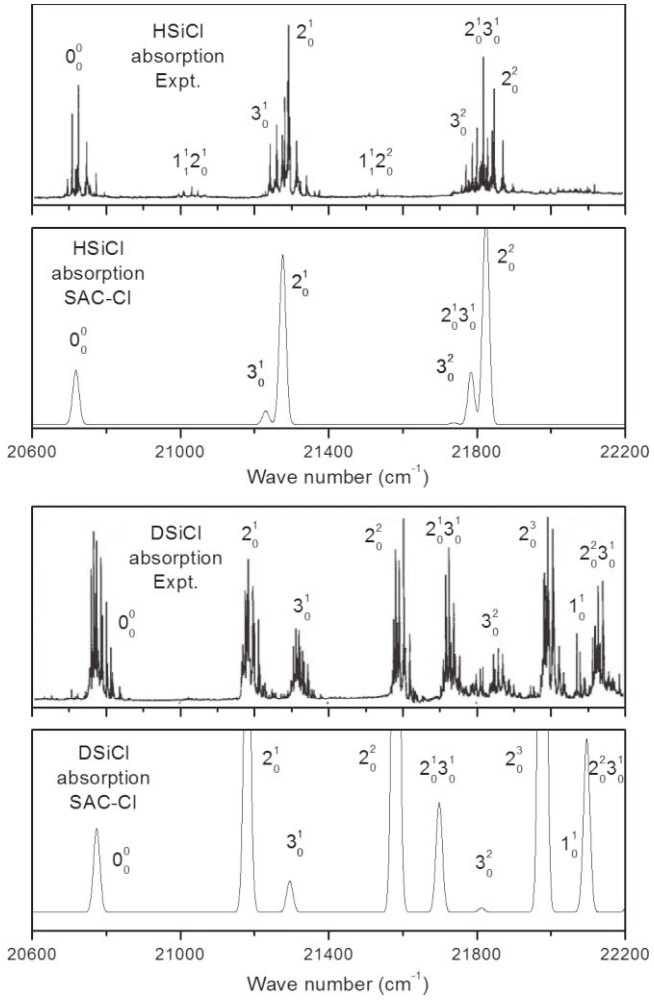

FIG. 5. The SAC–CI $X(000)$ absorption spectra of HSiCl and DSiCl compared with the observed LIF absorption spectra (Ref. 21).

and DSiCl are compiled in Table S3 of the supplementary material.[45]

The present simulations of the vibronic level emission and absorption spectra show that the SAC/SAC–CI PESs are accurate and well balanced in the ground and excited states.

D. HNO and HPO

The HNO and HPO molecules also have isovalence electronic structures to HSiF; the valence electronic structure of HNO in the ground state is $\ldots(6a')^2(1a'')^2(7a')^2(3a'')^0$. The results of the geometrical parameters and adiabatic excitation energies in the ground and singlet/triplet excited states of these molecules are summarized in Table VI with the experimental values[42,46,47] and previous theoretical results.[28,48] Luna *et al.*[28] investigated these electronic states by CASPT2 with the extensive ANO-type basis set [6*s*5*p*4*d*3*f*/5*s*4*p*3*d*2*f*/3*s*2*p*1*d*]. For T_0 of the A^1A'' state, the SAC/SAC–CI calculations with cc-pVTZ–f have provided excellent values of 1.646 and 2.346 eV for HNO and HPO, respectively, in comparison with experimental values of 1.631 (Ref. 46) and 2.360 eV.[47] The CASPT2 calculation[28] underestimated these energies by about 0.2 eV. For T_0 of the a^3A'' state, the present calculations have underestimated the experimental value by about 0.07 eV for HNO and have yielded a lower value for HPO compared with the QCISD(T) calculation with 6–311+G(3*df*,2*p*).[48]

For the geometry changes in the A^1A'' and a^3A'' states, the present calculations support the CASPT2 results. The calculated bond-angle change of the A^1A'' state is different between these two molecules; the bond angle of HPO decreases, in contrast to other molecules with this isovalence electronic structure. Although the experimental bond angle is 105.0° for A^1A'', theories predicted smaller angles of 93.3° by SAC–CI and 95.3° by CASPT2.[28] For a^3A'', the calculated bond angles are larger at 118.1° and 110.3° for HNO and HPO, respectively. The geometry changes in bond distances of HNO and HPO are also different from those of HCX and HSiX (X = F, Cl). The NO (PO) bond is elongated in A^1A'' by +0.03 (+0.09) Å, in reasonable agreement with the experiment and the previous CASPT2 calculation. This feature of the bond-distance change has also been found in the a^3A'' state.

The harmonic vibrational frequencies of these states have also been calculated and summarized in Table VII together with other theoretical[28] and experimental values.[42,46,47] In

TABLE VI. Geometries and adiabatic excitation energy (eV) of the ground and excited states of HNO and HPO calculated by the direct SAC–CI SD–*R* method with cc-pVTZ–f basis sets.

State	Method	r_{HA} (Å)	r_{AO} (Å)	Θ (°)	T_0
		HNO			
X^1A'	CASPT2[a]	1.056	1.214	108.1	...
	SAC–CI	1.051	1.210	107.9	...
	Expt. (r_0,θ_0)[b]	1.063(2)	1.212(1)	108.6(2)	...
A^1A''	CASPT2[a]	1.038	1.239	115.7	1.449
	SAC–CI	1.034	1.241	114.6	1.646
	Expt. (r_0,θ_0)[b]	1.0360(5)	1.241(1)	116.25(4)	1.631
a^3A''	CASPT2[a]	1.027	1.229	109.0	0.586
	SAC–CI	1.023	1.229	118.1	0.707
	Expt.[b]	...	...	...	0.781
		HPO			
X^1A'	CASPT2[a]	1.452	1.490	104.1	...
	SAC–CI	1.460	1.493	104.3	...
	Expt. (r_0,θ_0)[c]	1.456(3)	1.480(5)	103.5(25)	...
A^1A''	CASPT2[a]	1.45	1.573	95.3	2.087
	SAC–CI	1.451	1.585	93.3	2.346
	Expt. (r_0,θ_0)[c]	1.51(1)	1.549(3)	105(1)	2.360
a^3A''	CASPT2[a]	1.442	1.519	111.8	1.467
	QCI[d]	1.429	1.551	106.2	1.922
	SAC–CI	1.428	1.530	110.3	1.646

[a]Reference 28.
[b]Reference 46.
[c]Reference 47.
[d]Reference 48.

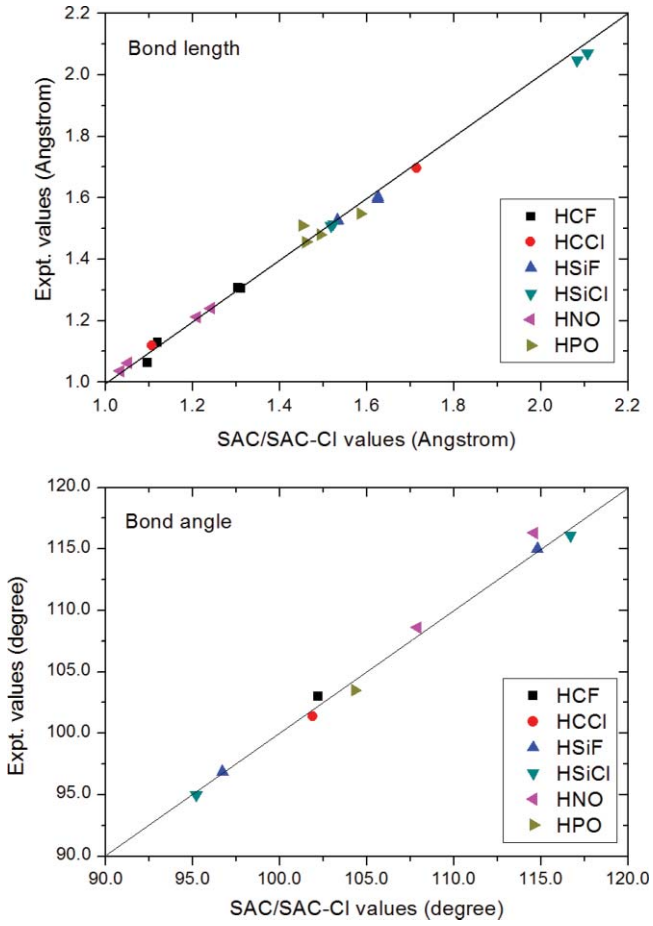

FIG. 6. Comparison of bond length (Å) and bond angle (°): theoretical vs. experimental values.

the CASPT2 calculations, the vibrational frequencies were evaluated by the second-degree polynomial fitting of the PESs.[28] The experimental values are fundamental vibrational frequencies and, therefore, theoretical vibrational frequencies including anharmonicity can be compared. In HNO, the ν_2 and ν_3 vibrational frequencies in both the A^1A'' and a^3A'' states are smaller than the respective frequencies in the ground state because the NO bond length is elongated and the bond angle becomes larger in the excited states. This agrees with the experimental measurement. The ν_1 value, on the other hand, becomes larger because the HN distance is decreased. The deviations of the vibrational frequencies from the experimental values are larger in HNO than those in HSiX or HCX molecules; the mean deviation was 45 cm^{-1} for the X^1A' and A^1A'' states.

The agreement with experiment is also reasonable for HPO. For example, the vibrational frequencies in the ground state were calculated to be 2056 (ν_1), 995 (ν_2), and 1205 (ν_3) cm^{-1}, in comparison with the experimental values, 2095 (ν_1), 998 (ν_2), and 1188 (ν_3) cm^{-1},[46] respectively; the deviations from the experimental values are 39, 3, and 17 cm^{-1}, respectively. In the A^1A'' state, the experimental ν_2 and ν_3 values have been reported as 566 and 858 cm^{-1},[42] respectively, and the present calculations yield the values as 635 and 878 cm^{-1}, respectively. No experimental data exist for the vibrational frequencies in the a^3A'' state; however, the present results are in agreement with those by the CASPT2 values.

The calculated vibrational frequencies of DNO and DPO within the BO approximation are summarized in Table VIII. Experimental values have been reported for the X^1A', A^1A'', and a^3A'' states of DNO and for the X^1A' and A^1A'' states of DPO. The trend of the vibrational frequencies in the ground and excited states of DNO (DPO) and the deviations from the experimental values are almost parallel to those of HNO (HPO). The calculated values show fair agreement with the experimental values. For instance, the calculated ν_2 and ν_3 are 782 and 1426 cm^{-1} (expt. 755 and 1401 cm^{-1}) for DNO and those for DPO are 478 and 867 cm^{-1} (expt. 438(5) and 846(5) cm^{-1}).

The calculated vibrational energies of the lowest 20 vibrational levels and their assignments for HPO and DPO are summarized in the supplementary material of Table S4.[45] For HNO and DNO, the photoelectron spectra of HNO^- and DNO^- have been observed[49] and a detailed theoretical analysis will be reported in a separate note.[50]

E. Comparison with experimental values

To evaluate the performance of the SAC–CI SD–*R* nonvariational calculations with cc-pVTZ–f basis sets for the equilibrium geometries, adiabatic excitation energies, and vibrational frequencies, the theoretical and experimental values are compared in Figs. 6 and 7. Note that the experimental values

TABLE VII. Harmonic and anharmonic vibrational frequencies (cm^{-1}) of the ground and excited states of HNO and HPO calculated by the direct SAC–CI SD–*R* method with cc-pVTZ–f basis sets.

State	Method	ω_1 (HN/HP)	ω_2 (bend)	ω_3 (NO/PO)	ν_1 (HN/HP)	ν_2 (bend)	ν_3 (NO/PO)
				HNO			
X^1A'	CASPT2[a]	2778	1474	1526	…	…	…
	SAC–CI	2991	1585	1630	2731	1543	1601
	Expt. (gas)[b]	…	…	…	2684	1501	1565
	Expt. (Ar)[b]	…	…	…	2716	1505	1563
A^1A''	CASPT2[a]	3184	975	1442	…	…	…
	SAC–CI	3201	1033	1480	2946	1016	1444
	Expt. (gas)[b]	…	…	…	2854	982	1421
	Expt. (Ar)[b]	…	…	…	…	982	1422
a^3A''	CASPT2[a]	3471	1026	1530	…	…	…
	SAC–CI	3380	1081	1571	3162	1051	1540
	Expt. (gas)[b]	…	…	…	…	992(150)	1468(140)
				HPO			
X^1A'	CASPT2[a]	2096	977	1115	…	…	…
	SAC–CI	2142	1015	1218	2056	995	1205
	Expt. (Ar)[b]	…	…	…	2095	998	1188
	Expt. (gas)[b]	…	…	…	…	986	1188
A^1A''	CASPT2[a]	1971	521	896	…	…	…
	SAC–CI	2118	654	886	1962	635	878
	Expt. (gas)[b]	…	…	…	…	566	858
a^3A''	CASPT2[a]	2245	617	1088	…	…	…
	SAC–CI	2266	571	1056	2137	555	1028

[a]Reference 28.
[b]Fundamental frequencies taken from Ref. 42.

have uncertainty and some values were reported about three decades ago. The results of the bond lengths and bond angles for all of the molecules considered in the present work, that is, HCF, HCCl, HSiF, HSiCl, HNO, and HPO, are compared with the experimental values in Fig. 6. The deviations from the line show the differences from the experimental values. Those of the vibrational frequencies and adiabatic excitation energies are shown in Fig. 7. In general, the agreement is excellent for HSiF (DSiF) and HSiCl (DSiF), whose experimental values were observed in recent works.[20,22] The deviations are relatively large for HCCl, HNO (DNO), and HPO (DPO). Experimental errors might also exist, however, for the values of HNO (DNO) and HPO (DPO); a method with higher accuracy seems to be necessary.

TABLE VIII. Vibrational frequencies of the ground and excited states of DNO and DPO calculated by the SAC–CI SD–*R* method with cc-pVTZ–f basis sets.

Molecule	State	Method	ν_1(HA)	ν_2(bend)	ν_3(AX)
DNO	X^1A'	SAC	2055	1182	1587
		Expt. (Ar) [a]	2043	1153	1547
		Expt. (gas)[a]	2025	…	1546
	A^1A''	SAC–CI	2233	782	1426
		Expt. (gas)[a]	2176	755	1401
	a^3A''	SAC–CI	2371	808	1525
		Expt. (gas)[a]	…	750(140)	1452(140)
DPO	X^1A'	SAC	1505	747	1203
		Expt. (Ar)[a]	1530	750	1186
		Expt. (gas)[a]	…	745	1177
	A^1A''	SAC–CI	1443	478	867
		Expt. (gas)[a]	…	438(5)	846(5)
	a^3A''	SAC–CI	1562	421	1019

[a]Fundamental frequencies taken from Ref. 42.

The overall mean deviations from the experimental values are 0.015 Å for HA bond length, 0.018 Å for AO bond length, 0.6° for bond angle, and 0.069 eV for adiabatic excitation energy except for the apparently different values such as the bond angle of HPO in the A^1A'' state. For the vibrational frequency, the mean deviation for HCF, HCCl, HSiF, HSiCl, and their isotopomers is 11.9 cm^{-1} and that for HNO, HPO, and their isotopomers is 37.7 cm^{-1}.

IV. PERTURBATION SELECTION WITH LMOs

In the SAC–CI method, perturbation selection[13] is effective for large-scale calculations on biological compounds and material-related molecules. The LMOs are effective for calculating the electron correlations and perturbation selection is effective with the use of LMOs. Various approaches of the local-correlation methods have been developed to calculate the electron correlations efficiently. However, in such cases, the PES may not be continuous and a singularity of the energy derivatives may appear. The MOD method[30] has been developed for calculating the analytical energy gradients in a singularity-free manner. Therefore, perturbation selection based on the LMOs combined with the MOD method is expected to be a rigorous method for the analytical energy gradients of the SAC/SAC–CI method. We have applied this

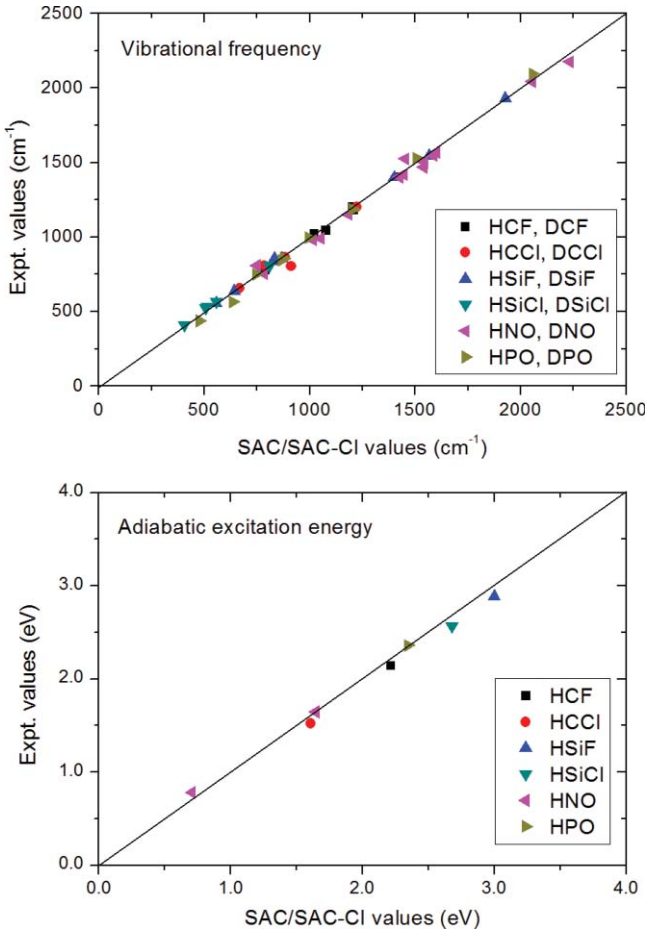

FIG. 7. Comparison of vibrational frequency (cm^{-1}) and adiabatic excitation energy (eV): theoretical vs. experimental values.

method to examine its effect on the geometrical parameters, total energy, and harmonic vibrational frequencies.

The present calculations of the equilibrium geometry and harmonic vibrational frequencies were performed in the following sequence.

1. The SAC–CI calculation was conducted with the LMOs and perturbation selection was performed. Pipek–Mezey population localization[32] was used for calculating the LMOs.
2. During the geometry optimization, the MOD method was applied and the sets of excitation operators were fixed to those at the initial geometry. The "MacroIteration" was repeated until the forces and geometry parameters converged.
3. The harmonic vibrational frequencies were calculated from the second derivatives numerically computed with the analytical first derivatives. In this step, the MOD method was used with excitation operators being unchanged. For this purpose, the group sum (GSUM) option was used in the GAUSSIAN09 program. By using GSUM option, the excitation operators were fixed at the starting geometry and the summation of operators was not taken.

The initial structures of the geometry optimization were set to those obtained by the full calculations. In the present calculation, the "MacroIteration" was used and the dependence of the results on the initial geometry was small.

The results for the X^1A', A^1A'', and a^3A'' states of HSiF are summarized in Table IX with the deviations from the values obtained by the full calculations without perturbation selection. We have examined some thresholds in the perturbation selection; e.g., $\lambda_g = 10^{-7}$, 10^{-8}, and 10^{-9} for SAC and the corresponding thresholds, $\lambda_e = 10^{-8}$, 10^{-9}, and 10^{-10}, respectively, for SAC–CI. The results with canonical MOs are also given in supplementary material of Table S5.[45] The convergence of the results using LMOs is faster than those using canonical MOs considering the SAC/SAC-CI dimensions, in particular, for the vibrational frequency. The effect of LMOs, however, is not so prominent for small molecules. In the calculations with LMOs, the deviations in the A^1A'' state for example, are 3.12, 1.13, and 0.54 mhartree for $\lambda_e = 10^{-8}$, 10^{-9}, and 10^{-10}, respectively. The errors in the transition energies from the full calculations are much small; for example, in the

TABLE IX. Errors in the calculations of geometrical parameters, total energies (ΔE, mhartree), transition energy ($\Delta\Delta E$, eV), and harmonic vibrational frequencies (cm^{-1}) of HSiF by the direct SAC–CI SD–*R* method with the perturbation selection based on LMOs. The deviations from the full calculations are given.

State	λ_g, λ_e	Dimension	Δr_{HA} (Å)	Δr_{AX} (Å)	$\Delta\theta$ (°)	ΔE (mh)	$\Delta\Delta E$ (eV)	$\Delta\omega_1$(HSi)	$\Delta\omega_2$(bend)	$\Delta\omega_3$(SiF)
X^1A'	10^{-7}	10292	0.003	0.001	0.0	4.38	...	17	129	11
	10^{-8}	15355	0.000	0.000	0.0	1.26	...	11	48	1
	10^{-9}	18569	0.000	0.000	0.0	0.37	...	2	15	0
		(40185)[a]								
A^1A''	10^{-7}, 10^{-8}	9592	0.003	0.001	0.4	3.12	0.034	16	47	0
	10^{-8}, 10^{-9}	13090	0.002	0.000	0.1	1.13	0.004	16	44	2
	10^{-9}, 10^{-10}	15668	0.000	0.000	0.0	0.54	0.005	2	19	1
		(40185)[a]								
a^3A''	10^{-7}, 10^{-8}	11182	0.003	0.001	0.2	3.94	0.011	36	133	32
	10^{-8}, 10^{-9}	16491	0.001	0.000	0.1	1.39	0.004	13	61	5
	10^{-9}, 10^{-10}	20661	0.000	0.000	0.0	0.47	0.003	7	22	1
		(56118)[a]								

[a]Dimension without perturbation selection.

a^3A'' state, deviations are 0.011, 0.004, and 0.003 eV for $\lambda_e = 10^{-8}$, 10^{-9}, and 10^{-10}, respectively. The convergence of the geometrical parameters is very fast and a reliable structure with errors less than 0.003 Å can be obtained in the lowest level of calculations ($\lambda_g = 10^{-7}$). On the other hand, the convergence of the harmonic vibrational frequencies is relatively slow, in particular for the bending mode, which is a soft coordinate. However, it is much faster than the calculations with canonical MOs. The convergence of the harmonic frequencies in the symmetric (ω_1, HSi) and antisymmetric (ω_3, SiF) modes is relatively fast.

The results for some other molecules in the present study also show similar trends. The present method, the perturbation-selection scheme using LMOs, is useful for geometry optimization to calculate the ground- and excited-state equilibrium geometries; however, it should be carefully used for calculations of the harmonic vibrational frequencies at the equilibrium geometries.

V. SUMMARY

In this work, the analytical energy gradients of the direct SAC–CI SD–*R* nonvariational method have been applied to calculate the excited-state equilibrium geometries and vibrational frequencies of the valence excited states of bent HAX-type molecules. For calculating the harmonic vibrational frequencies, the second derivatives have been computed numerically using the analytical first derivatives. The 3D PESs around the local minima were used to evaluate the anharmonicity of the vibrational frequencies.

The calculations have been performed for the lowest singlet and triplet states (A^1A'' and a^3A'') of HCX (X = F, Cl), HSiX (X = F, Cl), and HAO (A = N, P), some of which have been well studied by high-resolution spectroscopy and *ab initio* calculations. The vibrational analysis has also been performed for these molecules and their isotopomers, DCX (X = F, Cl), DSiX (X = F, Cl), and DAO (A = N, P). The calculated results show good agreement with the available experimental values and other theoretical values, which show the reliability of the method. The vibrational level emission spectra of HSiF and DSiF and absorption spectra of HSiCl and DSiCl were simulated within the FC approximation. The peak positions and relative intensities of the vibrational peaks were well reproduced, which show the well-balanced description of the ground and excited states by the SAC/SAC–CI method. The geometry changes in the excited states are interpreted based on the electrostatic theory using the electron density difference between the ground and excited states.

Geometry optimization using perturbation selection combined with the MOD method and LMOs is shown to be effective for calculating the excited-state geometry. However, it should be carefully used for calculating the harmonic vibrational frequencies, in particular for soft modes such as bending and torsion coordinates.

ACKNOWLEDGMENTS

This study was supported by JST-CREST, a Grant-in-Aid for Scientific Research from the Japanese Society for the Promotion of Science (JSPS) and the Ministry of Education, Culture, Sports, Science, and Technology (MEXT) of Japan and the Next Generation Supercomputing Project. The computations were partly performed using the Research Center for Computational Science in Okazaki, Japan.

[1] S. D. Peyerimhoff, Adv. Quantum Chem. **9**, 69 (1975); R. J. Buenker and S. D. Peyerimhoff, Theor. Chim. Acta **12**, 183 (1968).
[2] H. Nakatsuji and K. Hirao, J. Chem. Phys. **68**, 2053 (1978).
[3] H. Nakatsuji, Chem. Phys. Lett. **59**, 362 (1978); **67**, 329 (1979).
[4] H. Nakatsuji, Acta Chim. Hung.-Models in Chemistry **129**, 719 (1992).
[5] H. Nakatsuji, J. Chem. Phys. **83**, 713 (1985); D. Mukherjee and S. Pal, Adv. Quantum Chem. **20**, 291 (1989); X. Li and J. Paldus, J. Chem. Phys. **107**, 6257 (1997).
[6] K. Andersson, P.-A. Malmqvist, B. O. Roos, A. J. Sadlej, and K. Wolinski, J. Phys. Chem. **94**, 5483 (1990).
[7] K. Hirao, Chem. Phys. Lett. **190**, 374 (1992).
[8] M. Ehara, J. Hasegawa, and H. Nakatsuji, *SAC-CI Method Applied to Molecular Spectroscopy, in Theory and Applications of Computational Chemistry: The First 40 Years, A Volume of Technical and Historical Perspectives* (Elsevier, Oxford, 2005).
[9] T. Nakajima and H. Nakatsuji, Chem. Phys. Lett. **280**, 79 (1997); Chem. Phys. **242**, 177 (1999).
[10] M. Ishida, K. Toyota, M. Ehara, H. Nakatsuji, and M. J. Frisch, J. Chem. Phys. **120**, 2593 (2004).
[11] J. A. Pople, M. Head-Gordon, and K. Raghavachari, J. Chem. Phys. **87**, 5968 (1987).
[12] N. C. Handy, J. A. Pople, M. Head-Gordon, K. Raghavachari, and G. W. Trucks, Chem. Phys. Lett. **164**, 185 (1989).
[13] H. Nakatsuji, Chem. Phys. **75**, 425 (1983).
[14] R. Fukuda and H. Nakatsuji, J. Chem. Phys. **128**, 094105 (2008).
[15] J. M. Bowman, S. Carter, and X. Huang, Int. Rev. Phys. Chem. **22**, 533 (2003).
[16] R. B. Gerber and J. O. Jung, in *Computational Molecular Spectroscopy*, edited by P. Jensen and P. R. Bunker (Wiley, New York, 2000).
[17] O. Christiansen, J. Chem. Phys. **120**, 2140 (2004).
[18] S. Maeda, Y. Watanabe, and K. Ohno, J. Chem. Phys. **128**, 144111 (2008).
[19] W. W. Harper, D. A. Hostutler, and D. J. Clouthier, J. Chem. Phys. **106**, 4367 (1997).
[20] D. A. Hostutler, D. J. Clouthier, and R. H. Judge, J. Chem. Phys. **114**, 10728 (2001).
[21] W. W. Harper and D. J. Clouthier, J. Chem. Phys. **106**, 9461 (1997).
[22] D. A. Hostutler, N. Ndiege, D. J. Clouthier, and S. W. Pauls, J. Chem. Phys. **115**, 5485 (2001).
[23] D. K. W. Mok, E. P. F. Lee, F. Chau, and J. M. Dyke, J. Chem. Phys. **120**, 1292 (2004).
[24] D. K. W. Mok, E. P. F. Lee, F. Chau, and J. M. Dyke, J. Chem. Theory Comput. **5**, 565 (2009).
[25] T. W. Schmidt, G. B. Bacskay, and S. H. Kable, Chem. Phys. Lett. **292**, 80 (1998).
[26] C. F. Rodriquez and A. C. Hopkinson, J. Phys. Chem. **97**, 849 (1993).
[27] G. E. Scuseria, M. Duran, R. G. A. R. Maclagan, and H. F. Schaefer III, J. Am. Chem. Soc. **108**, 3248 (1986).
[28] A. Luna, M. Merchan, and B. O. Roos, Chem. Phys. **196**, 437 (1995).
[29] H. Nakatsuji, J. Am. Chem. Soc. **95**, 345 (1973); H. Nakatsuji and T. Koga, *The Force Concept in Chemistry* (Van Nostrand Reinhold, New York, 1981).
[30] K. Toyota, M. Ehara, and H. Nakatsuji, Chem. Phys. Lett. **356**, 1 (2002); K. Toyota, M. Ishida, M. Ehara, M. J. Frisch, and H. Nakatsuji, *ibid.* **367**, 730 (2003).
[31] T. H. Dunning, Jr., J. Chem. Phys. **90**, 1007 (1989).
[32] J. Pipek and P. G. Mezey, J. Chem. Phys. **90**, 4916 (1989).
[33] M. H. Beck and H.-D. Meyer, J. Chem. Phys. **114**, 2036 (2001); S. Carter and N. C. Handy, Mol. Phys. **57**, 175 (1986).
[34] G. A. Worth, M. H. Beck, A. Jackle, and H.-D. Meyer, The MCTDH package, version 8.3, Heidelberg University, Germany, 2003.
[35] M. J. Frisch, G. W. Trucks, H. B. Schlegel *et al.*, GAUSSIAN09, Revision B.01, Gaussian, Inc., Wallingford, CT, 2010.
[36] T. Suzuki and E. Hirota, J. Chem. Phys. **88**, 6778 (1988).
[37] T. Suzuki, S. Saito, and E. Hirota, J. Mol. Spectrosc. **90**, 447 (1981).
[38] M. Kakimoto, S. Saito, and E. Hirota, J. Mol. Spectrosc. **88**, 300 (1981).

[39]M. Kakimoto, S. Saito, and E. Hirota, J. Mol. Spectrosc. **97**, 194 (1983).
[40]A. J. Merer and D. N. Travis, Can. J. Phys. **44**, 525 (1966).
[41]W. A. Gilchrist, E. Reyna, and J. B. Coon, J. Mol. Spectrosc. **74**, 345 (1979).
[42]M. E. Jacox, J. Phys. Chem. Ref. Data **17**, 269 (1988).
[43]S. G. Lias, J. E. Bartmess, J. F. Liebman, R. D. Levin, and W. G. Mallard, J. Phys. Chem. Ref. Data **17**, Supplement 1 (1988).
[44]Z. K. Ismail, L. Fredin, R. H. Hauge, and J. L. Margrave, J. Chem. Phys. **77**, 1626 (1982).
[45]See supplementary material at http://dx.doi.org/10.1063/1.3617233 for the vibrational levels of HCF, DCF, HCCl, DCCl, HSiCl, DSiCl, HPO, and DPO calculated by the SAC-CI 3D PESs. The examination of perturbation selection with canonical MOs is also given.
[46]F. W. Dalby, Can. J. Phys. **36**, 1336 (1958).
[47]M. Larzilliere, N. Damany, and L. Thanh My, Chem. Phys. **46**, 401 (1980).
[48]M. Esseffar, A. Luna, O. Mo, and M. Yanez, Chem. Phys. Lett. **209**, 557 (1993).
[49]H. B. Ellis Jr. and G. B. Ellison, J. Chem. Phys. **78**, 6541 (1982).
[50]M. Ehara, T. Miyahara, and H. Nakatsuji, "Photodetachment spectra of HNO and DNO anions studied by the analytical energy gradients of SAC-CI method" (unpublished).